Bulletin of the
Seismological Society of America

Vol. 72 April 1982 No. 2

DYNAMIC FAULTING STUDIED BY A FINITE DIFFERENCE METHOD

BY JEAN VIRIEUX AND RAUL MADARIAGA

ABSTRACT

We have developed a finite difference method that is especially adapted to the study of dynamic shear cracks. We studied a number of simple earthquake source models in two and three dimensions with special emphasis on the modeling of the stress field. We compared our numerical results for semi-infinite and self-similar shear cracks with the few exact solutions that are available in the literature. We then studied spontaneous rupture propagation with the help of a maximum stress criterion. From dimensional arguments and a few simple examples, we showed that the maximum stress criterion depended on the physical dimensions of the fault. For a given maximum stress intensity, the finer the numerical mesh, the higher the maximum stress that had to be adopted. A study of in-plane cracks showed that at high rupture velocities, the numerical results did not resolve the stress concentration due to the rupture front from the stress peak associated with the shear wave propagating in front of the crack. We suggest that this is the reason why transonic rupture velocities are found in the numerical solutions of in-plane faulting when the rupture resistance is rather low. Finally, we studied the spontaneous propagation of an initially circular rupture. Two distinct modes of nucleation of the rupture were studied. In the first, a plane circular shear crack was formed instantaneously in a uniformly prestressed medium. After a while, once stress concentrations had developed around the crack edge, the rupture started to grow. In the second type of nucleation, a preexisting circular crack became unstable at time $t = 0$ and started to grow. The latter model appeared to us as a more realistic simulation of earthquake triggering. In this case, the initial stress was nonuniform and was the static field of the preexisting fault.

INTRODUCTION

The rupture process at the source of shallow earthquakes may be approximately modeled by the spontaneous propagation of a dynamic shear crack. In dynamic models, the prestress field and rock mechanical properties determine the slip between the walls of the fault and the progression of the rupture front. A shear crack in a prestressed medium creates a shear-stress drop, and the propagation of rupture is controlled by a certain rupture criterion which depends on the strength of the rocks in the vicinity of the rupture front. A simplified model, in which slip is controlled by stress drop but the movement of the rupture front is prescribed as a function of time, is frequently used. In this paper, we shall deal mainly with fully dynamic, spontaneous rupture in two and three dimensions, and we shall compare our results with those of the simpler, fixed-rupture velocity models.

Crack problems, especially fully dynamic ones, are very difficult to solve. For this reason, only a few simple geometrical models have been solved analytically, e.g., the elliptical self-similar crack studied by Kostrov (1964), Burridge and Willis (1969),

and Richards (1973, 1976). The antiplane dynamic shear crack was studied by Kostrov (1966), who gave a closed solution for a semi-infinite crack. Practically all the other available solutions have been obtained by numerical methods. The two-dimensional problem was solved both by Burridge (1969) and Das and Aki (1977) by a numerical solution of boundary integral equations and by Shmuely and Alterman (1973), Andrews (1976), Stockl (1977), and others by numerical finite difference methods. Archuleta and Day (1980) and Das (1980) have studied three-dimensional shear cracks by finite elements and boundary integral equations, respectively. Spontaneous three-dimensional solutions have been proposed by Day (1979), Das (1981), and Miyatake (1980). A major difficulty with three-dimensional numerical solutions is the need of a large computer capacity. Some authors avoided this problem by studying models possessing a certain symmetry, as Madariaga (1976) did in the case of circular cracks or by making some approximations (Mikumo and Miyatake, 1979) in order to reduce the three-dimensional problem to a two-dimensional one.

In this paper, we present a new numerical finite difference method for the solution of spontaneous dynamic shear cracks. The method is similar to the one used previously by Madariaga (1976) for the solution of circular cracks. A modification in the way boundary conditions are imposed on the crack significantly improves the stability of the solutions, especially the stress on the fault plane. This allows us to use the maximum stress criterion of Das and Aki (1977) and Shmuely and Peretz (1976) in the study of spontaneous rupture.

The Crack and Its Numerical Solution

Let us consider an infinite, linear elastic medium subject to a static prestress, $\tau_{xz} = \sigma_0(x, y, z)$. At time $t = 0$, a crack starts to propagate on the plane (x, y) such that on the newly fractured area, the shear traction τ_{xz} drops to the dynamic friction σ_f and, simultaneously, a displacement discontinuity, or slip, appears across the fault plane. Our purpose is to calculate the slip given σ_0 and σ_f as functions of position on the crack and time.

We have to solve numerically the elastodynamic equations of motion for a uniform medium

$$\begin{aligned} \rho \dot{u}_i &= \tau_{ij,j} \\ \tau_{ij} &= \lambda u_{k,k}\delta_{ij} + \mu(u_{i,j} + u_{j,i}) \end{aligned} \tag{1}$$

where ρ, λ, and μ are the density and elastic constants of the medium. u_i and τ_{ij} are the displacements and incremental stresses measured with respect to the initial prestressed configuration. δ_{ij} is Kronecker's delta. Dots indicate time derivatives, commas partial differentiation with respect to the space component indicated by the index following the comma.

We have found (Madariaga, 1976) that imposing boundary conditions is much simpler when the second-order partial differential equation (1) is transformed into the following system of nine first-order equations

$$\begin{aligned} \rho \dot{v}_i &= \tau_{ij,j} \\ \dot{\tau}_{ij} &= \lambda v_{k,k}\delta_{ij} + \mu(v_{i,j} + v_{j,i}) \quad \text{for} \quad i \geqq j. \end{aligned} \tag{2}$$

Here, v_i is the particle velocity. Crack problems are mixed-boundary value problems

since they require stress conditions inside the crack and fixed velocity outside the crack. These boundary conditions are easily found using symmetry properties about the crack plane. Let S_1 be the crack at time t and S_2 the rest of the fault plane outside the crack. The boundary conditions for a plane shear crack are

$$v_x = v_y = 0 \quad \text{on} \quad S_2 \tag{3a}$$

and

$$\begin{aligned} \tau_{xz} &= -\sigma_0 \approx \sigma_e \cos(\psi) \\ \tau_{yz} &= -\sigma_f \sin(\psi) \end{aligned} \qquad \text{on } S_1 \tag{3b}$$

where $\sigma_e = \sigma_0 - \sigma_f$ is the effective stress, and ψ is the angle of slip with respect to the x axis, and

$$\tau_{zz} = 0 \qquad \text{on both } S_1 \text{ and } S_2. \tag{3c}$$

In order to make explicit the dependence of the solution on the source parameters, we use nondimensional variables defined by

$$\begin{aligned} \tau_{ij} &= \sigma_e T_{ij} \\ (x, y, z) &= L(X, Y, Z) \\ t &= L/c, t' \\ v_i &= \sigma_e c/m V_i \\ u_i &= \sigma_e L/m U_i. \end{aligned} \tag{4}$$

L is a characteristic length of the problem, i.e., the grid step d for a self-similar or semi-infinite crack, or the length of a finite crack. c is either α, P-wave velocity, for three-dimensional and plane cracks, or β, S-wave velocity, for antiplane cracks. m is either $(\lambda + 2\mu)$ for three-dimensional and plane cracks, or μ for antiplane cracks. In all of our calculations, we have assumed that $\lambda = \mu$.

We find the following normalized system

$$\begin{aligned} \dot{V}_i &= T_{ij,j} + C\nabla^2 V_i \\ \dot{T}_{ij} &= \lambda/m V_{k,k}\delta_{ij} + \mu/m(V_{i,j} + V_{j,i}) \quad i \geqq j \end{aligned} \tag{5}$$

where we have added a viscous dissipation term to the equation for particle velocities. C is a nondimensional attenuation coefficient chosen so as to dissipate spurious high-frequency oscillations in the numerical solutions, generated by abrupt stress drop on the crack.

The Finite Difference Method

The main features of the numerical method were already exposed in Madariaga (1976): we try to build a grid to solve the normalized system of equations (5) by centered finite differences. Of the many ways to do that, we prefer the one that yields the simplest finite difference expressions. It turns out that this grid has also

the fewest number of grid points per finite difference cell. Let us consider the antiplane grid shown in Figure 1a. Introducing the notation

$$F(i\Delta y, j\Delta z, k\Delta t) = F(i, j, k) \tag{6}$$

where $y = i\Delta y$, $z = j\Delta z$, $t = k\Delta t$, and F is any of the variables of the problem. We may write the finite difference equivalent of equation (5)

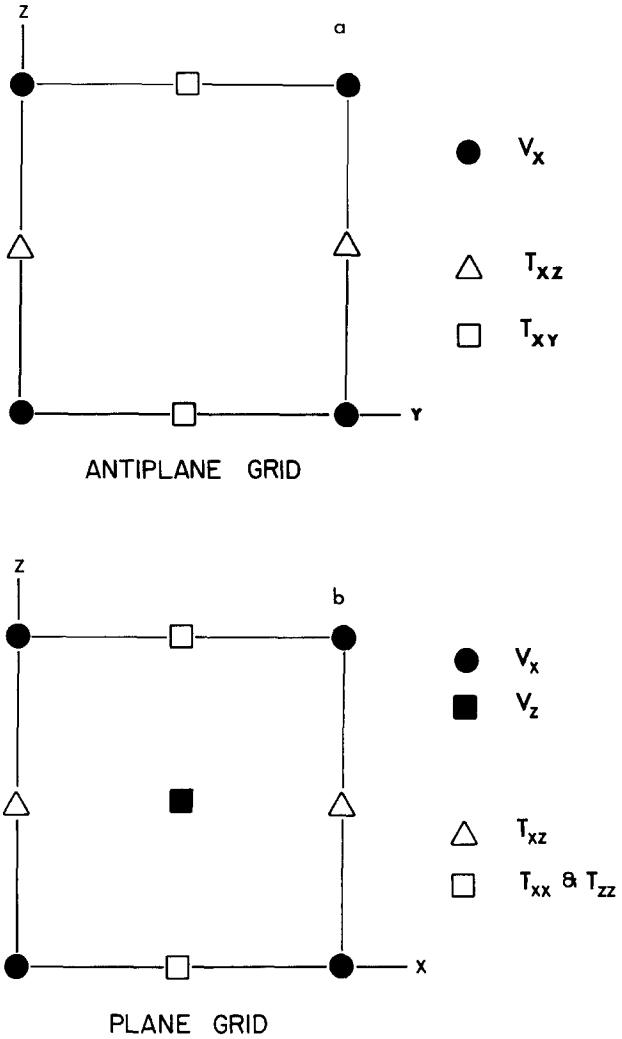

FIG. 1. (a) The numerical finite difference grid for antiplane elastodynamic problems. Two different times are shown on the same spatial grid: closed symbols are for time k and open symbols are for time $(k + \frac{1}{2})$. (b) Same as (a), but for in-plane elastodynamic problems.

$$V_x(i, j, k+1) = V_x(i, j, k) + \frac{\Delta t}{\Delta y}\left[T_{xy}(i+\tfrac{1}{2}, j, k+\tfrac{1}{2}) - T_{xy}(i-\tfrac{1}{2}, j, k+\tfrac{1}{2})\right]$$
$$+ \frac{\Delta t}{\Delta z}\left[T_{xz}(i, j+\tfrac{1}{2}, k+\tfrac{1}{2}) - T_{xz}(i, j-\tfrac{1}{2}, k+\tfrac{1}{2})\right]. \tag{7}$$

The damping term has been eliminated for simplicity. Thus, the method is explicit since the velocity V_x at $t = (k + 1)\Delta t$ is calculated from the velocity at $t = k\Delta t$ and

the stress at $t = (k + \frac{1}{2})\Delta t$. In fact, an examination of the system (5) shows that stresses are needed only at half-times $(k + \frac{1}{2})\Delta t$ and that, if we tried to calculate both stresses and velocities at the same time, we would have a system that would completely uncouple into several staggered schemes like the one we have just presented. We may now provide the equations for the stresses.

$$T_{xy}(i + \tfrac{1}{2}, j, k + \tfrac{1}{2}) = T_{xy}(i + \tfrac{1}{2}, j, k - \tfrac{1}{2}) + \frac{\Delta t}{\Delta y}[V_x(i + 1, j, k) - V_x(i, j, k)]$$

$$T_{xz}(i, j + \tfrac{1}{2}, k + \tfrac{1}{2}) = T_{xz}(i, j + \tfrac{1}{2}, k - \tfrac{1}{2}) + \frac{\Delta t}{\Delta z}[V_x(i, j + 1, k) - V_x(i, j, k)]. \quad (8)$$

The calculation is again explicit and we may combine the stress and velocity equations into a single explicit two-step finite difference method. The grid is completely staggered both in space and time and has a side-centered cubic symmetry.

Proceeding in the same way as above, we have found the grids for plane and three-dimensional elasticity shown in Figures 1b and 2, respectively. Both have the same properties described for the antiplane problem.

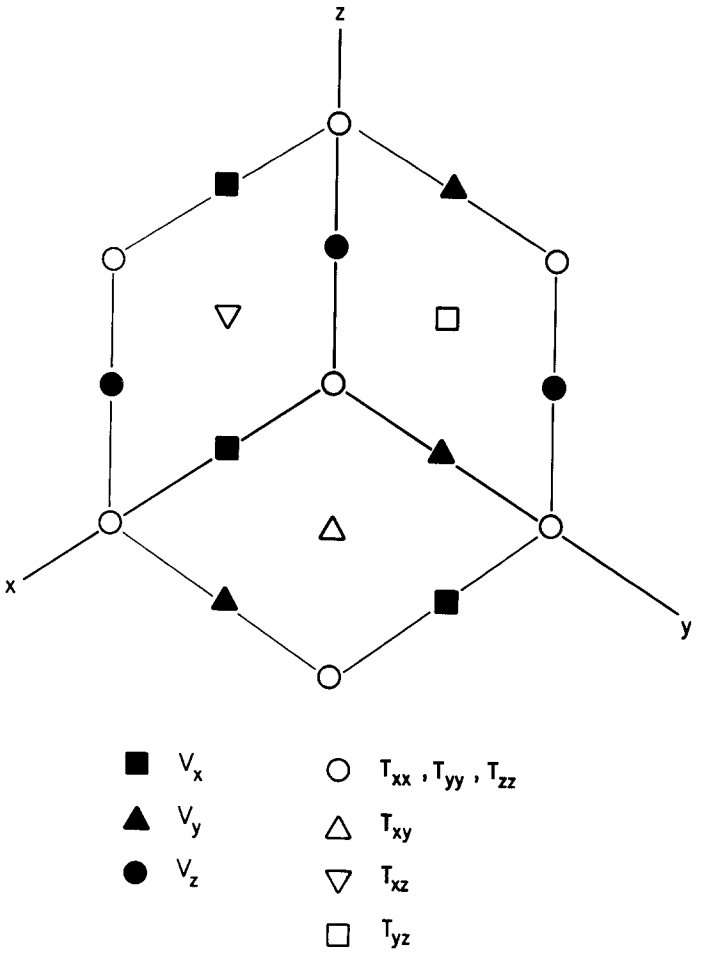

FIG 2. The numerical finite difference grid for three-dimensional elastodynamic problems.

Numerical stability may be found in the usual way (Alford *et al.*, 1974)

$$H + C < n^{-1/2} \tag{9}$$

where $n = 2$ or $n = 3$ for two- or three-dimensional problems, respectively. $H = \Delta t/\Delta x = \Delta t/\Delta y = \Delta t/\Delta z$ is the ratio between time increments and space grid steps. In most instances, we choose $H = 0.5$ for two-dimensional calculations and $H = 0.25$ for three-dimensional calculations. Since the P-wave velocity $\alpha = 1$ in the normalized equations, $H = 0.5$ means that the numerical information moves at a velocity $\Delta x/\Delta t$ which is twice the P-wave velocity. H is closely related to the numerical dispersion created by the discretization of the wave equation. Precision, on the other hand, is controlled by the number of points chosen to model a fault of given length. This poses a problem at the beginning of rupture since the initial crack will be modeled by a very small number of points, and the precision of the solution will be correspondingly poor. As the fault grows the number of points inside the crack increases and so does precision. The most severe source of problems with the numerical method comes from the discretization of the rupture front. The damping term characterized by the coefficient C reduces efficiently the oscillations coming from rapid stress changes; but the oscillations due to the propagation of the crack are not so well suppressed because they are continuously generated every time the rupture front advances by a grid step.

As in the case of the grid selection, we have several possible ways of implementing the boundary conditions [(3a) to (3c)]. Since the boundary conditions are mixed, we cannot specify V_y, V_x on S_2 and T_{zx}, T_{zy} on S_1 on the same numerical plane. This is an intrinsic property of finite difference methods for mixed-boundary value problems and requires the introduction of a ghost plane to satisfy the boundary conditions on S_1. In Madariaga (1976), the stress on the fault plane was specified via a ghost line. This method yields very stable estimates of slip velocity and is quite suitable to calculate seismic radiation from the fault by a representation theorem. Stresses on the fault plane are less reliable since we do not have stress directly calculated on the extension of the fault plane itself but on a plane slightly off (by $\Delta z/2$) from the fault. This smoothes the stress field in a way unsuitable for spontaneous rupture propagation.

A different implementation of the boundary conditions was introduced by Virieux (1979). Here the symmetry or antisymmetry of the field variables about the fault plane are exploited and shear stress is computed directly on the fault plane. Referring to Figure 2 and assuming that this represents a grid cell on the $z = 0$ boundary, the fault plane is taken as a plane normal to z through the center of the cell, i.e., a plane through T_{zx}, T_{yz}, and V_z. With this choice, the particle velocities V_x and V_y are calculated on a plane slightly off (by $\Delta z/2$) from the fault plane, and they are less reliably determined. On the other hand, the stresses T_{xz} and T_{yz} outside the crack and their singularities are better resolved. Since we are interested in spontaneous propagation, we have used this new procedure in the numerical calculation reported in this paper. The trade-off between stress and slip precision seems to be inherent in finite difference solutions to mixed-boundary value problems and stems from our inability to specify both velocity and shear stress on the same grid plane.

Antiplane Crack with Fixed Velocity

The first problem we shall consider is a semi-infinite antiplane crack that appears suddenly along the negative y axis at time $t = 0$, and then propagates at a constant

rupture velocity. This problem admits an exact solution that may be found using the method developed by Kostrov (1966). Das and Aki (1977) used this model, with rupture velocity $\beta/2$, as a test for their boundary-integral equation method. We shall perform here a similar test of our numerical method.

In Figure 3, a and b, we present the stress field and the displacement field at several positions along the crack axis. We see how the stress field grows as the usual inverse square-root singularity and drops abruptly once the rupture front arrives. Slip begins immediately after the passage of the rupture front and has a typical hyperbolic form. The exact solution is given by the continuous line, the numerical one is represented by the crosses. The crack slip is systematically underestimated; this comes from the fact that we calculate velocities and displacements not on the crack itself but half-a-space step away from the fault. This problem may not be

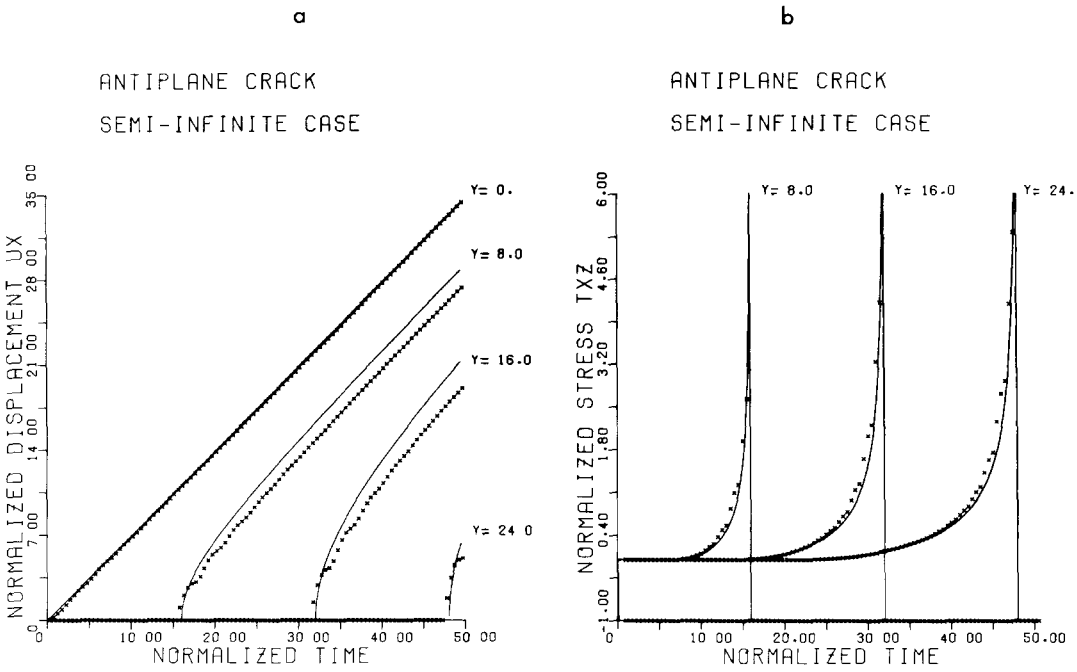

FIG 3. Stress and displacement history of a semi-infinite antiplane crack growing with fixed-rupture velocity $v = 0.5\,\beta$. Crosses indicate numerical solution, lines the analytical one. A very good resolution of the stress singularity is seen while there is a clear delay of the displacement. All variables are scaled as in equation (4) with L equal to the grid spacing d.

entirely eliminated since it comes from the way boundary conditions are applied on the grid; velocities and stresses are never calculated at the same points.

DYNAMIC ANTIPLANE CRACK

Spontaneous propagation from an instantaneously appearing semi-infinite crack. One of the goals of the development of numerical methods to solve crack problems is to study spontaneous rupture propagation in which the rupture history is not prespecified but is determined from material properties. Since we want to test the capabilities of our numerical method, we shall first study the only dynamic faulting problem that admits an exact solution: the semi-infinite, instantaneously appearing, antiplane fault model of Kostrov (1966). This same problem was studied numerically by Das and Aki (1977).

A major problem with rupture criteria is that they are based on the local stress and velocity field near the crack tips, and both fields have inverse square-root singularities. In numerical solutions, we are limited to a discrete approximation of these fields. We are thus forced to use a few points near the tip to introduce a criterion that will, hopefully, simulate the rupture criterion in the continuum. Several such criteria have been proposed in the literature; they may be classed into two types: the maximum stress criterion in which the node ahead of the crack tip is relaxed once the stress overcomes a certain maximum stress. This criterion has been used by Das and Aki (1977), Shmuely and Peretz (1976), and Owen and Shantaram (1977), among others. Alternatively, a numerical version of the energy release rate may be used; here, several of the points near the crack tip are used to calculate the energy flow into the rupture front (Owen and Shantaram, 1977; Popelar and Gehlen, 1979).

The stress field we have calculated for the fixed-velocity models presented in the previous section is sufficiently accurate and stable in order to attempt a simulation of spontaneous crack growth. We have tested both the maximum stress and energy criteria (Virieux, 1979) but we shall concentrate here on the maximum stress criterion as applied to a semi-infinite antiplane crack. The crack extends initially between $-\infty < y < 0$ and, at time $t = 0$, it is loaded instantaneously with a uniform stress $\sigma_{xz} = -\sigma_e = \sigma_f - \sigma_0$. After a certain time t_c, the load on the crack tip is enough to start rupture which accelerates eventually to the shear velocity. This problem admits an exact solution obtained by the method of Kostrov (1966). Assuming that the rupture criterion is that the stress intensity factor should be constant and equal to k_t, we find that the crack tip position is given by

$$\begin{aligned} y_c &= 0 \qquad t \leqq t_c \\ y_c &= \beta(t - t_c) - \beta t_c \log(t/t_c) \qquad t > t_c \end{aligned} \tag{10}$$

where $t_c = \pi^2 k_t^2 / 4\beta\sigma_e^2$.

Das and Aki (1977) have proposed that the maximum stress criterion is related to the constant k_t rupture model. Let σ_u be the maximum acceptable stress and σ_f the kinematic friction in the crack plane. Then, assuming that the crack tip is at the middle between two grid points, they found

$$\sigma_u - \sigma_f = 2k_t d^{-1/2} \tag{11}$$

where d is the grid spacing. Since σ_f and d are given, this is a linear relationship between σ_u and k_t. Introducing normalized variables and noting that k_t is normalized by $\sigma_e L^{1/2}$, we find

$$\frac{\sigma_u - \sigma_f}{\sigma_e} = 2K_t(L/d)^{1/2} \tag{12}$$

where K_t is the nondimensional stress intensity factor. Using Das and Aki's notation

$$T_u = \frac{\sigma_u - \sigma_0}{\sigma_e}$$

we find

$$1 + T_u = 2K_t(L/d)^{1/2} \tag{13}$$

where T_u is the nondimensional maximum stress increase measured from the initial stress.

In order to interpret numerical results in terms of physical variables, we have to fix the length scale. For the semi-infinite crack that we study in this section, we choose $L = d$, the grid spacing. In this case

$$1 + T_u = 2K_t \tag{14}$$

with

$$K_t = k_t/(\sigma_e d^{1/2})$$

as shown by Das and Aki (1977). It should be noted, however, that this semi-infinite crack problem does not have an intrinsic length scale. It is precisely this lack of scale that allows its exact solution. An alternative choice to $L = d$ would be to take $L = \beta\, t_c$ with t_c defined by (10).

In Figure 4, we present crack tip trajectories calculated for the semi-infinite, instantaneous antiplane crack. The results are labeled according to the nondimensional stress intensity factor K_t used in the numerical solution. We have recalculated the value of K_t adjusting the analytical solution to the numerical one by means of a least-squares fit. We obtain in this way an adjusted stress intensity factor K_c which is also given in the figures. The analytical solutions are given by the continuous lines while the numerical solution is marked by crosses. We have repeated the preceding calculation with another grid ratio $H = 0.25$. We find practically the same results which indicate that the numerical dispersion does not have a major influence on the determination of rupture propagation.

From our numerical results, we have found a good agreement between analytical and numerical solutions for

$$2 < K_t < 4 \quad \text{or} \quad 3 < T_u < 7. \tag{15}$$

The lower limit is probably due to the poor resolution of the stress concentration in the vicinity of the crack tip. The critical stress intensity is too low and the numerically computed stress intensity too high; as a result, the numerical solution accelerates faster than the analytical one. Let us note that this limit $T_u = 3$ is larger than the maximum stress increase allowed in most numerical simulations that have appeared in the literature (Das and Aki, 1977; Das, 1981; Day, 1979; Miyatake, 1980). The upper limit of K_t corresponds to a high rupture resistance. In this case, the numerical solution seems to have some difficulty in building up the stress concentration. This is probably due to smoothing of the stress field near the crack tip.

Since rupture propagation is controlled by the local stress field near the rupture front, we shall assume that the limits for K_t found above will also apply to finite cracks provided that a proper scaling of these limits is taken into account, i.e.,

$$2\sqrt{d/L} < K_t < 4\sqrt{d/L} \tag{16}$$

where as before $K_t = k_t/(\sigma_e L^{1/2})$. These limits to the applicability of the numerical rupture criterion are intimately related to the properties of our numerical method. It may happen that the other numerical methods proposed in the literature have different limits of applicability.

Spontaneous propagation from a finite initial crack. The problem of crack nucleation is very important in simulating earthquake faulting. The semi-infinite model studied in the previous section is very unsatisfactory in this respect since it has no counterpart in three dimensions. For this reason we shall study the nucleation of rupture from a finite initial crack. Two models shall be considered; in the first, the crack is loaded by prestress and has reached the critical stress criterion at time

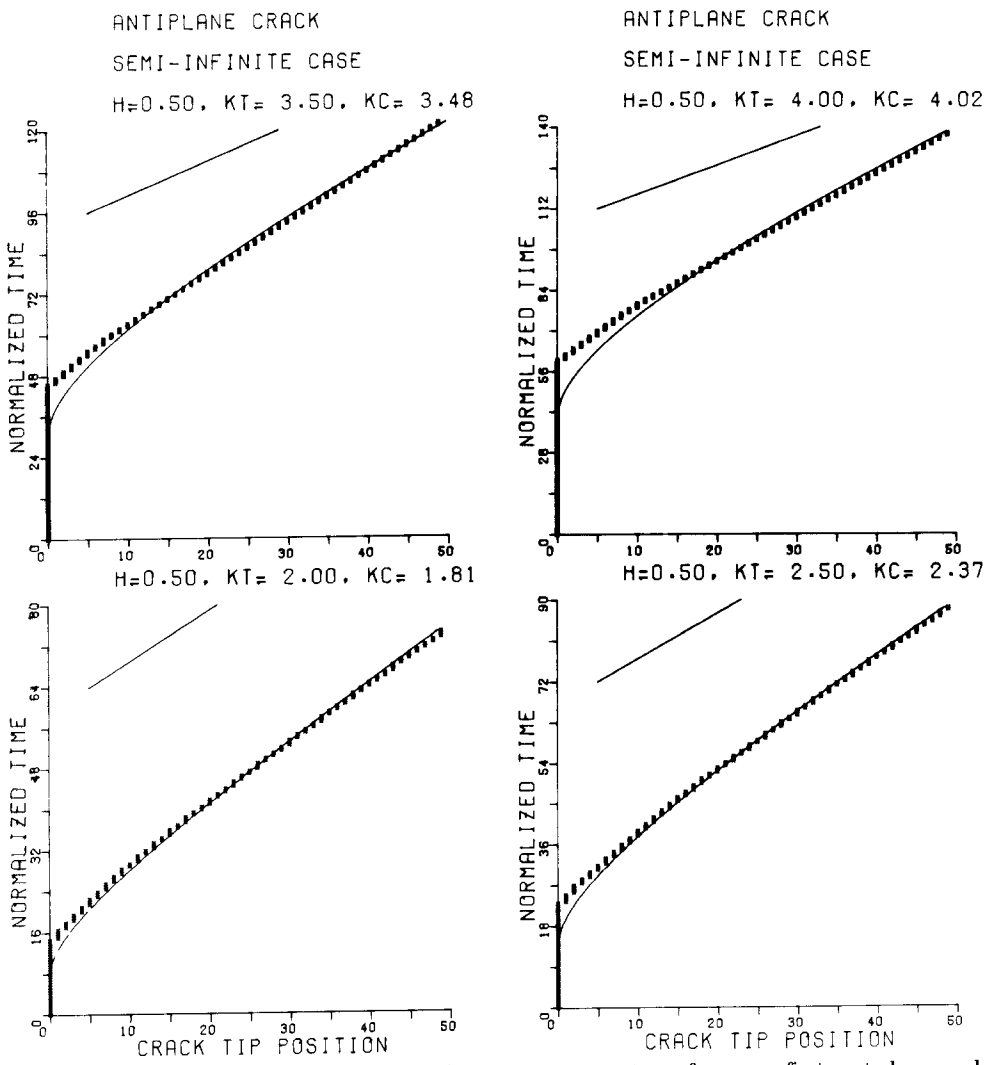

FIG. 4. The motion of the crack tip during the spontaneous rupture of a semi-infinite antiplane crack The crosses describe the numerical position of the crack tip for several values of the nominal stress intensity K_I. Lines are adjusted analytical crack tip position for the recalculated stress intensity K_c. Rupture velocity β is shown for comparison. Scaling length is the grid spacing d

$t = 0$. In the second case, the finite crack is loaded instantaneously at time $t = 0$ by a uniform initial stress. The latter model is less physically satisfactory than the first one, but it is cheaper to solve and has been used to start rupture in three dimensions by Das (1981) and Miyatake (1980). The first case is more expensive to solve since it requires calculating the initial prestress field. The static prestress is obtained using the viscous damping term to reduce oscillations. Once the velocity field is everywhere negligible, we consider that we have reached the static limit.

In order to solve the preexisting crack model, we take an initial crack of 40 grid points. We use the initial crack half-length as the scale length: $L = 20\ d$. From the static prestress solution, we find the nondimensional stress intensity factor

$$K_t = 0.686$$

which is well within the limits, 0.447 and 0.894 given by equation (16) since $(d/L)^{1/2} = 20^{-1/2}$. The preexisting crack is initially in metastable equilibrium, and in order to start rupture, we relax the grid points just in front of the crack tips. The crack becomes unstable and propagates symmetrically until it triplicates its initial length; then it stops abruptly. We have assumed that the interior of the preexisting crack is not locked; we found that a substantial amount of slip takes place there. In Figure 5a, we show the propagation of the crack tip as a function of time. Rupture

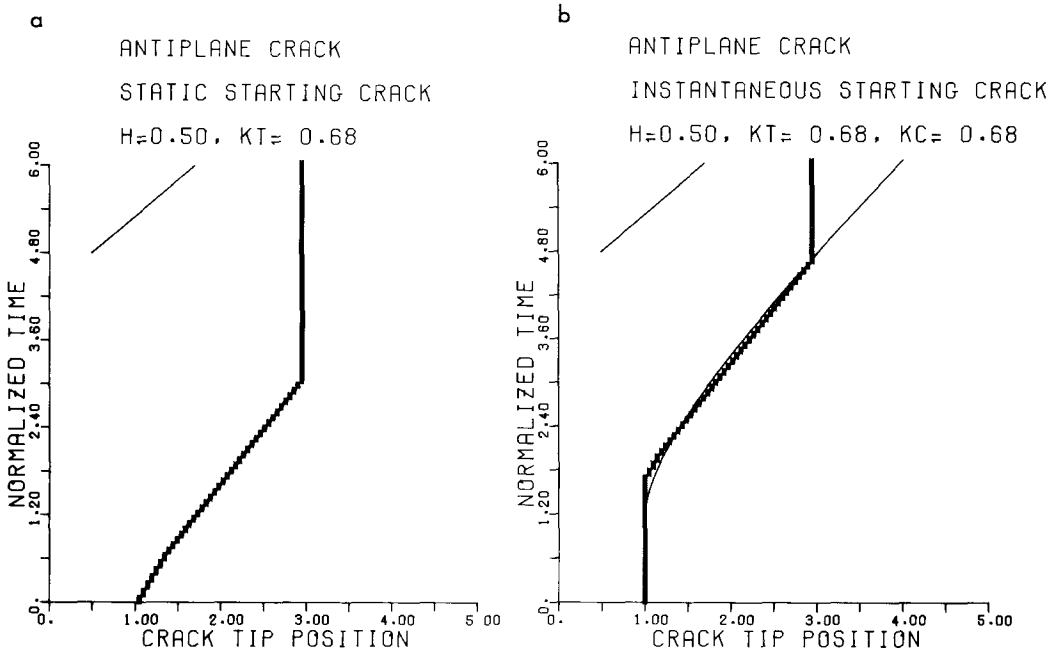

FIG 5 (a) Spontaneous rupture of a preexisting finite antiplane crack Numerical crack tip position is plotted against time The crack is loaded by static prestress and becomes unstable at $t = 0$ K_t is the static stress intensity factor. The crack stops when it triplicates its initial length The scaling length is the initial crack length (b) Spontaneous rupture of an instantaneously loaded finite antiplane crack. Numerical crack tip position is plotted against time. The crack waits for a time t_c to overcome the critical stress intensity K_t and start propagating. It stops when it triplicates its initial length The line is the analytical semi-infinite antiplane crack tip position for the recalculated stress intensity K_c Length scale is the size of the initial crack.

starts immediately at $t = 0$ and, after a period of acceleration which is faster than in the case of the semi-infinite crack, the crack reaches a velocity of 0.66 β just before rupture arrest.

The stress field T_{xz} on the crack and its extension is shown in Figure 6a at equally spaced instants of time. The maximum stress T_u related to $K_t = 0.686$ by (13) is then $T_u = 5.136$. We see that during propagation, T_{xz} is usually lower than this value, except just before the crack jumps by a grid step. After the crack stops growing, a much higher stress singularity develops in front of the crack tip. The slip inside the crack is given in Figure 6b at the same times for which T_{xz} is shown in Figure 6a. Let us note that slip is measured from the initial state at $t = 0$ and not from a

completely relaxed state before the introduction of the preexisting crack. The slip in Figure 6b presents two distinct features: the large elliptical slip function due to the new rupture and the central slip deficiency due to the preexisting crack. If we added the preslip in the central part of the fault, we would find a simple elliptical slip. In this case, we would be measuring the total slip with respect to an initial completely relaxed stress field. We should remark that from purely seismological measurements, we would not be able to detect this initial preslip (or antidislocation in the terms introduced by Andrews, 1974). As the new crack becomes longer, the initial slip becomes smaller and smaller with respect to the total slip.

In the second model that we shall discuss in this section, we consider a finite crack of half-length $L = 20\ d$, appearing instataneously at time $t = 0$ and propagating spontaneously with the rupture criterion $K_t = 0.686$. Before interaction between the

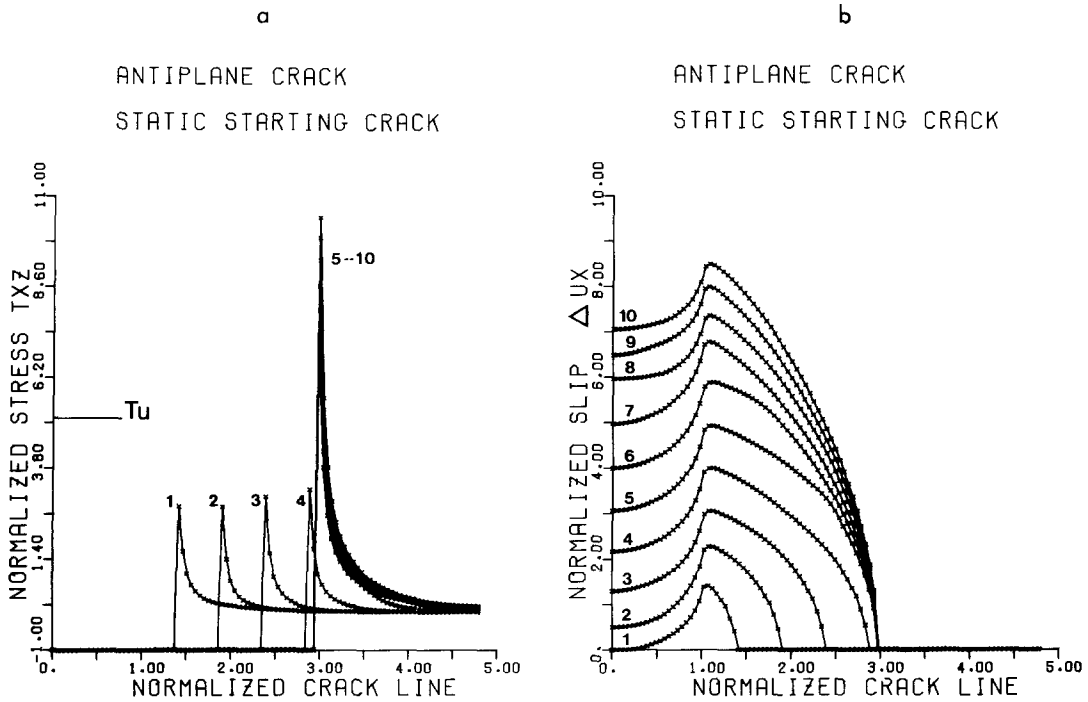

FIG. 6. Numerical solution for the spontaneous antiplane crack of Figure 5a Stress and slip fields on the crack line are shown at 10 different normalized times starting from 0.75 with a step of 0.75 T_u is the maximum stress associated with the static stress intensity K_t. Scale length is the initial length of the crack.

two crack tips, this model closely corresponds to the semi-infinite crack studied in the previous section. The crack tip trajectory is shown in Figure 5b. As in the semi-infinite case, a certain time close to t_c of equation (10) elapses before the rupture starts to grow. During this time, the stress concentration builds up in front of the crack tip until it reaches the rupture criterion $K_t = 0.686$. It is remarkable that the crack may start to grow with this value of K_t which corresponds to the stress intensity factor of the static crack. This indicates that the dynamic stress intensity for instantaneous loading overshoots the static stress intensity. After the initial acceleration, rupture velocity reaches $0.66\ \beta$ before the crack is stopped abruptly at $L_f = 60\ d$. The stress field, shown in Figure 7a, is very similar to the stress field for the preexisting crack of Figure 6a. The slip shown in Figure 7b, on the other hand, is different from that in Figure 6b since the slip deficiency due to the preexisting

crack has now disappeared. After the crack has started to grow, slip is very similar to the elliptical slip function of the self-similar crack (Kostrov, 1964). Once the crack stops, slip continues for a while until the arrival of the healing phases. Simultaneously, the stress concentration builds up outside the crack and, as expected, it reaches a similar value to that of the example in Figure 6a.

Returning to the case of the preexisting crack, we see that the final stress concentration, once the crack has ceased to grow, is much higher than the concentration at the beginning of rupture. This shows that for a fixed-effective stress drop σ_e, the stress intensity depends on the square root of the crack length, i.e.,

$$k_t = 0.686\ \sigma_e L^{1/2} \tag{17}$$

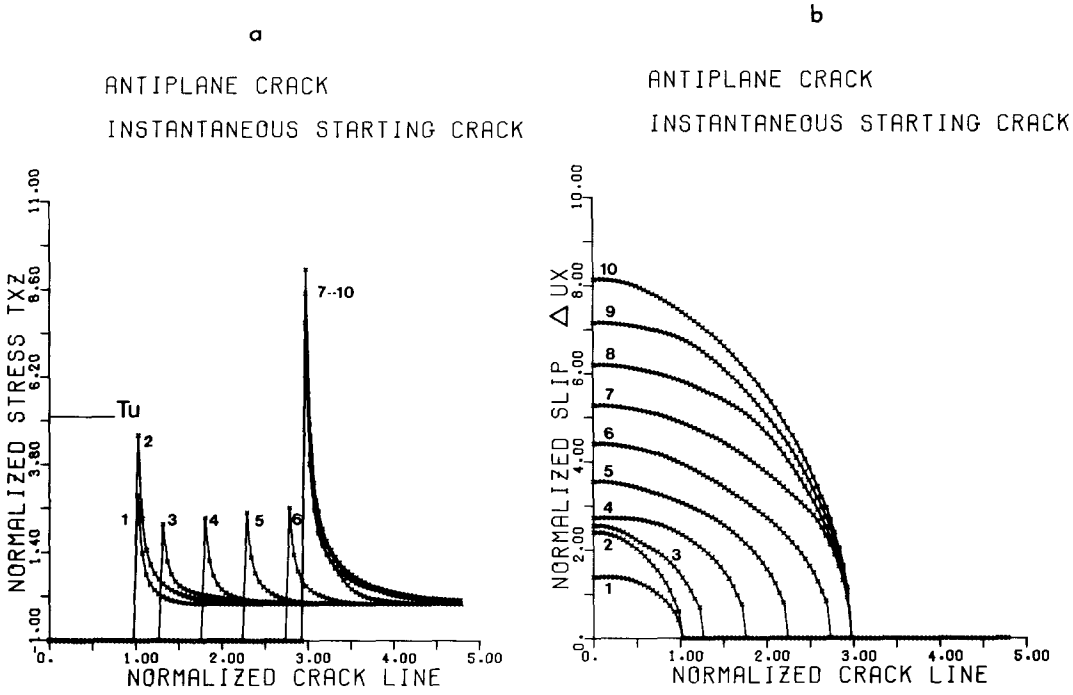

FIG 7. Numerical solution for the spontaneous antiplane crack of Figure 5b. Stress and slip fields on the crack line are shown at 10 different normalized times starting from 0.75 with a step of 0.75 T_u is the maximum stress associated with the static stress intensity K_t Scale length is the initial length of the crack.

in both cases. Initially $L = L_0 = 20\ d$, while at the end of rupture $L = L_f = 60\ d$. When normalizing length by $L_0 = 20\ d$, the stress intensity at the end of rupture is $3\frac{1}{2}$ times larger than that at the beginning. If we renormalized the final stress field with the new scale length, $L_f = 60\ d$, we would obtain the same results as in the initial preexisting crack, except that now we would have a much denser grid and a better resolution of the stress field near the crack tip. The whole process may be now restarted, and we may repeat the rupture simulation. This clearly shows that the numerical criterion depends on the number of points used to model the crack: if we increase the number of points from L_0 to L_f, the rupture criterion has to be correspondingly increased by $(L_f/L_0)^{1/2}$.

SELF-SIMILAR IN-PLANE SHEAR CRACK

In-plane shear crack problems are much more difficult to solve analytically than antiplane problems because of the coupling between P and SV waves. The only

problem for which a complete analytical solution is available is the self-similar in-plane shear crack. In this model, a crack appears at time $t = 0$ at the origin of coordinates and then propagates bilaterally with fixed-rupture velocity along the x axis. The crack plane is thus the x-y plane, and the crack extends indefinitely in the y direction. A uniform shear prestress field σ_0 exists before rupture. Once the rupture starts, the stress inside the cracked part of the x axis drops to the frictional stress σ_f. A solution to this problem for subsonic rupture velocities was found by Kostrov (1964) who showed that the slip inside the crack is given by

$$\Delta u_x(x, y) = C\,\sigma_e/\mu\,\sqrt{v^2t^2 - x^2} \qquad vt > |x| \tag{18}$$

where C is a numerical constant. Using (18) as a dislocation distribution, the stress in the fault plane was calculated by Cagniard-de Hoop's method.

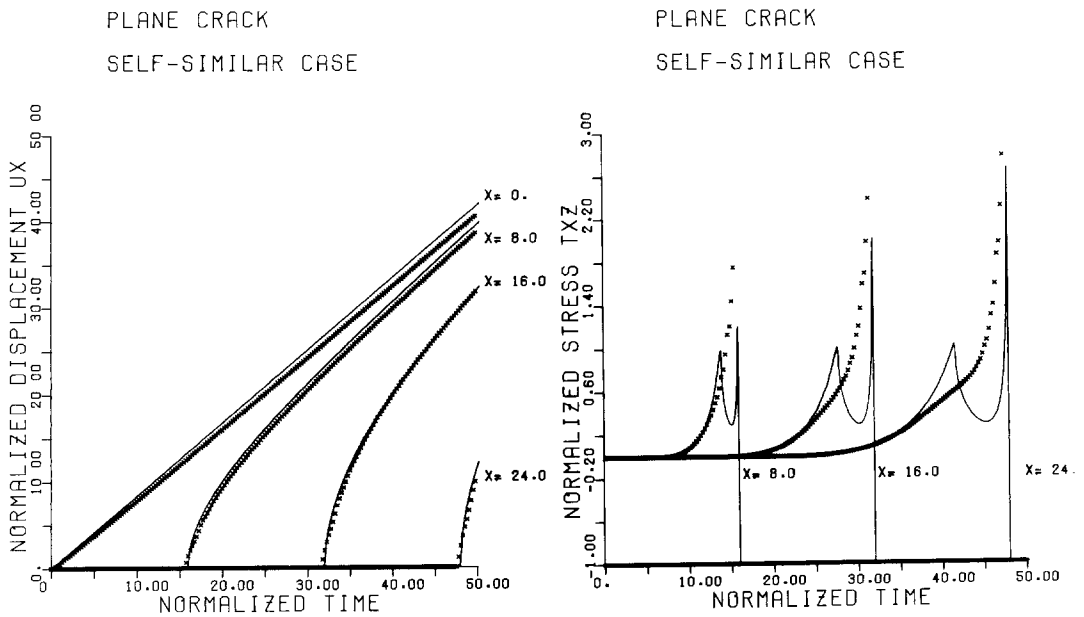

FIG. 8. Stress and displacement history of a self-similar in-plane crack growing at fixed-rupture velocity $v = 0.5\,\alpha$. Crosses indicate numerical solution, lines the analytical one. The numerical stress singularity averages the shear-stress peak associated with the S wave and the crack tip stress singularity. The displacement has clear delay with respect to the exact solution. Scale length is the grid spacing d.

Let us now solve the self-similar in-plane crack by means of our numerical method. The self-similar problem, as evidenced by the slip function (18), has no intrinsic length scale. For this reason, we choose the grid spacing d as the length scale in our solution. The rest of the variables are scaled as described in "The Crack and Its Numerical Solutions."

We have studied the stress and displacement field of the self-similar crack for a rupture velocity $v = 0.86\,\beta$ or $v = 0.5\,\alpha$. The U_x component of the displacement field and the T_{xz} component of the stress field at several positions along the x axis are shown in Figures 8 as a function of time. The continuous line shows the exact analytical solution, while the crosses represent the numerical results. The displacement U_x follows very closely the analytical solution: it is zero before the arrival of the rupture front and then increases hyperbolically as predicted by the theoretical result (18). The numerical solution is slightly delayed with respect to the analytical one because displacements are not calculated exactly on the crack but slightly off it.

We consider that the numerical displacement U_x is very satisfactory and so is the slip function ΔU_x.

The stress field on the other hand is not so well modeled by the numerical solution. In particular, the peak associated with the S wave is not present in the numerical result. Only a slight bump begins to form at $X = 24$. In our opinion. this problem is due to the numerical smoothness of our boundary conditions, inducing an averaged representation of the elastic fields (especially the T_{zz} field) around the crack tip, and so a rather smooth emission of shear waves. The numerical solution lacks enough resolution and, as seen in Figure 8, the stress field ahead of the crack only crudely approximates the exact stress field, averaging the stress concentration due to the rupture front and the S-wave peak. The numerical stress concentration is wider and more important than the analytical stress concentration.

Spontaneous In-Plane Shear Crack

In this section, we shall study the spontaneous growth of an in-plane crack under the same rupture criterion that we used for the antiplane case. First, we shall concentrate upon the validity of this criterion by studying the spontaneous semi-infinite crack. Then, we shall present results for a spontaneous finite crack.

Let a semi-infinite crack appear instantaneously at time $t = 0$ along the negative x axis. The material is under an uniform prestress field σ_0. Inside, the crack stress drops instantaneously to σ_f, the dynamic frictional stress. As in the antiplane case, the stress intensity factor ahead of the crack will grow until it reaches the critical value k_t. At that time, t_c, the crack will start to grow accelerating to a terminal velocity that depends on the value of k_t, and the grid spacing through the expression of the normalized stress intensity factor $K_t = k_t/(\sigma_e d^{1/2})$.

We do not have an analytical solution of this problem so that we shall only display numerical results. In Figure 9, we show the crack tip position as a function of time for four different values of K_t. Assuming that the results of the antiplane case do apply to the in-plane one, we restricted our study to $2 < K_t < 4$. For $K_t < 2.5$, we found that the rupture velocity tends to the P-wave velocity; for instance, for $K_t = 2$, the limit velocity was $0.86\ \alpha$. At $K_t = 2.5$, we encounter a transition zone in which the rupture front transverses very slowly the Rayleigh wave velocity and then goes supersonic. For values of $K_t > 2.5$, the limiting rupture velocity is always lower than Rayleigh's. We assume an upper limit exists for K_t due to numerical dispersion close to $K_t = 4$, just as in the antiplane case. Thus, as long as $2.5 < K_t < 4$, the maximum rupture velocity is the Rayleigh wave velocity. For a finite fault of length L, the equivalent limits are

$$2.5\ \sqrt{d/L} < K_t < 4\ \sqrt{d/L}$$

where d is the grid spacing and K_t is normalized by $\sigma_e L^{1/2}$.

For values of $K_t < 2.5\ (d/L)^{1/2}$, the rupture front becomes transonic and approaches the P-wave velocity. This occurs in our opinion because as we showed in the previous section, the numerical stress concentration represents the combination of the stress concentration itself and the S-wave stress peak. Theoretical solutions, on the other hand, separate the rupture front stress concentration from the S-wave peak. Only the rupture front stress concentration is used in the calculation of the maximum rupture velocity, which is invariably the Rayleigh velocity. In the numerical method, at high rupture velocities, the S-wave stress peak coalesces with the rupture front stress concentration. Strictly, then the equivalence between the "stress

intensity factor level criterion" and the "stress level criterion" based on an average of the elastic stress over the grid spacing d fails for values of $K_t < 2.5$.

Alternatively, we may, as Das and Aki (1977) proposed, interpret the numerical result as being due to the presence of a finite cohesive zone at the rupture front, i.e., in the numerical methods, the rupture front is not a point but a finite zone a few grid spaces long, say d'. The only problem then is the relation between d and d',

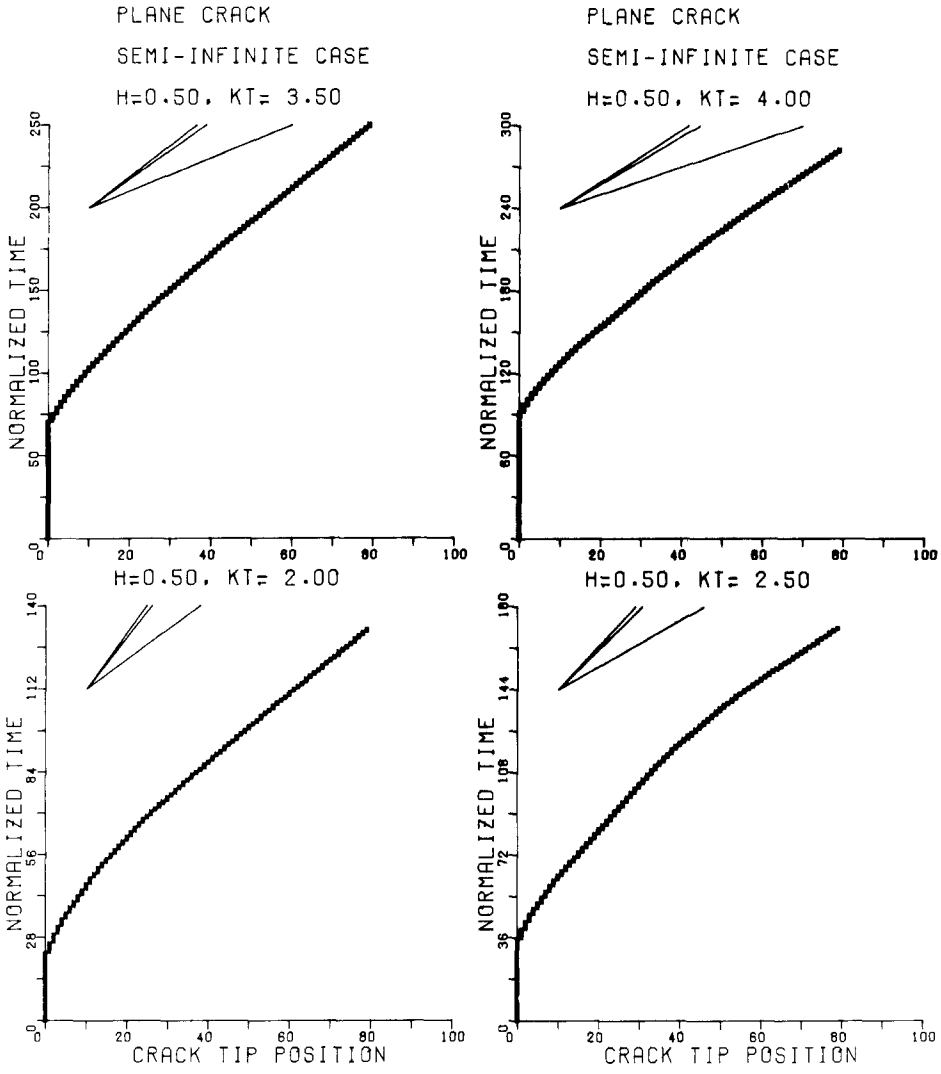

FIG 9. The motion of the crack tip during the spontaneous rupture of a semi-infinite in-plane crack. Crosses describe the numerical position of the crack tip for several values of the nominal stress intensity K_t. Ruptures velocity slopes α, β, and c_r are shown for comparison. Scale length is the grid spacing d.

necessary for a translation into physical terms. In terms of slip-weakening cohesive models in which the stress singularity is removed, it may be argued, as Andrews (1976) did, that for low values of stress level, the S-wave stress peak can break the material, allowing for transonic ruptures velocities. In any case, we conclude that the transonic rupture velocities are an intrinsic feature of our numerical method not related to oscillations or instabilities of the stress field but due to the numerical

coalescence of the strong S-wave peak ahead of the crack tip and the rupture front stress concentration.

Let us consider now a finite crack of half-length $L = 20\ d$ under an initial static loading. At time $t = 0$, the static critical stress intensity is reached, and the crack starts to grow spontaneously. Rupture growth is controlled then by the critical stress intensity $K_t = 0.59$. We stopped the crack abruptly when it triplicated its initial length. We present the numerical propagation of the crack tip in Figure 10. We notice that the rupture velocity is lower than the Rayleigh one, as expected for $K_t > 0.55$. The slip field ΔU_x and the stress field T_{xz} are presented in Figure 11 and show the same global features of the corresponding antiplane case. A strong S wave is emitted when the crack abruptly stops, inducing an S-wave peak in the stress field, in front of the stress singularity.

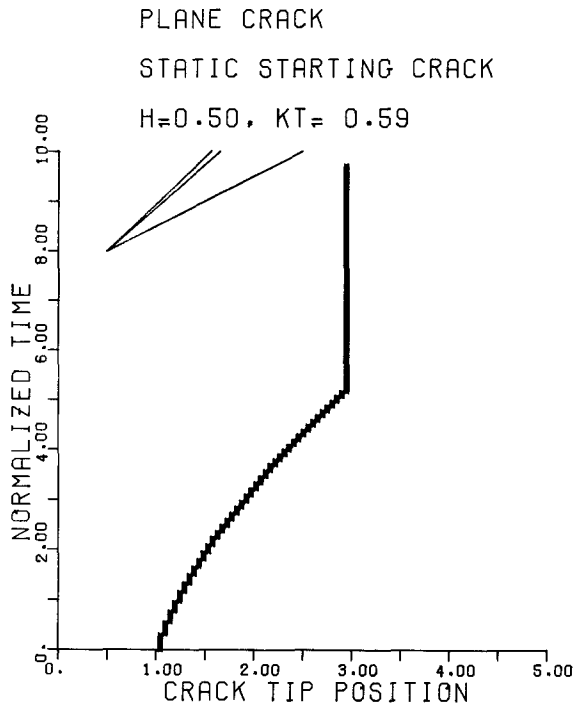

FIG 10. Spontaneous rupture of a preexisting finite in-plane crack. Numerical crack tip position is plotted against time. The crack is loaded by static prestress and becomes unstable at $t = 0$. K_t is the static prestress intensity factor. The crack stops when it triplicates its initial length. Rupture velocity slopes α, β, and c_r are shown for comparison.

DYNAMIC THREE-DIMENSIONAL SHEAR CRACKS

Let us consider now the spontaneous propagation of a planar shear crack in a prestressed three-dimensional medium. The implementation of a rupture criterion poses a number of problems since we are now in the presence of a mixed-rupture mode, with mode II (in-plane shear) and mode III (antiplane shear) stress concentrations. In order to translate a rupture criterion based on the stress intensities K_{II} and K_{III} into a maximum stress criterion, it is necessary to average the stress field over those grid element $d \times d$ which contain the rupture front. While in two dimensions we assumed that the rupture front was at the center of a grid interval, here we would have to assume the shape of the rupture front. We proceeded as follows: first, in order to simplify the calculations, we assumed that only the T_{xz}

component of the shear traction on the fault plane (x, y) presents a large stress concentration. T_{yz} should be small, a hypothesis that we have verified in our numerical calculations. If this hypothesis were not verified, we would have to decompose stress field near the rupture front into in-plane and antiplane shear components and apply a rupture criterion to each component. In fact, the rupture criterion for three-dimensional cracks is based on energy flow considerations, and there does not seem to be any easy way to express this criterion in terms of stress intensities. We shall therefore use a maximum stress intensity criterion on the T_{xz} stress component exclusively. Let K_t be this maximum intensity. We shall assume that the intervals of validity of the numerical criterion is the same as that determined for in-plane problem, i.e.,

$$2.5\sqrt{d/L} < K_t < 4\sqrt{d/L}$$

where L is a characteristic length.

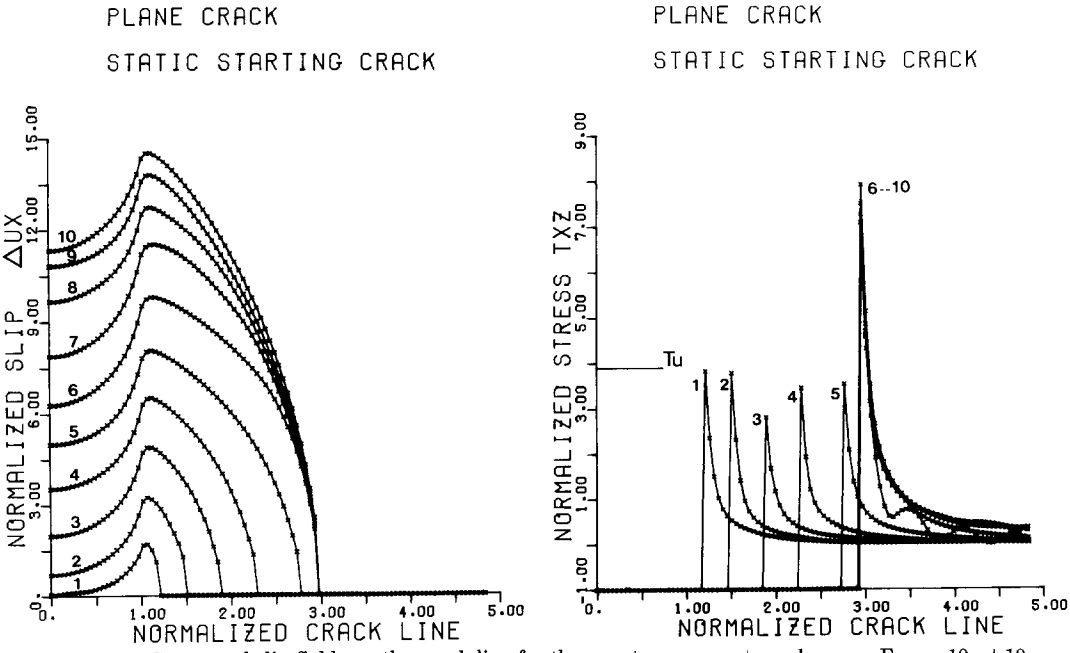

FIG. 11. Stress and slip fields on the crack line for the spontaneous rupture shown in Figure 10, at 10 different normalized times starting from 1 with a step of 1. T_u is the maximum stress associated with the static stress intensity K_t.

Spontaneous growth of a preexisting circular crack. Let us consider a static preexisting circular crack on the (x, y) plane of radius equal to 10 grid spacings ($L = 10\ d$). The crack has glided in response to a tectonic stress T_{xz} applied at infinity. Slip inside the crack has the typical ellipsoidal shape associated with penny-shaped cracks. The stress field has inverse square-root concentrations around the crack edges; the maximum normalized stress intensity is $K_t = 0.42$ along the x axis. The stress intensity is lower in the y direction as expected from theoretical considerations. We shall use $K_t = 0.42$ as the maximum admissible stress intensity. The problem at hand is similar to those treated in the sections on "Dynamic Antiplane Crank" and "Spontaneous In-Plane Shear Crack" for the antiplane and plane cases, respectively. The crack at time $t = 0$ is in metastable equilibrium, ready to start growing. In the two-dimensional cases, rupture was started relaxing the node in front of the crack

tip, the crack was then slightly longer and became unstable. In the circular case, the crack is locally metastable only along the x axis, i.e., in the pure in-plane direction. It is, however, stable along the y axis (pure antiplane direction). Strictly then, rupture should start from the in-plane direction, creating a highly asymmetrical rupture. Instead of this, we overdrove the stress concentration around the crack edges forcing it to increase its radius by one grid space, and then we let it grow spontaneously. The crack, after a brief arrest, starts to grow faster in the x direction (pure in-plane mode) than it does in the y direction as shown in Figure 12. We stop rupture abruptly once the half-length along the x direction is twice the initial crack radius (Figure 12). Just before crack arrest, the rupture velocity was $v = 0.45\ \alpha$ in the x direction and $v = 0.31\ \alpha$ in the y direction. We did not verify whether the crack would go transonic in the x direction since we did not let it grow long enough. In

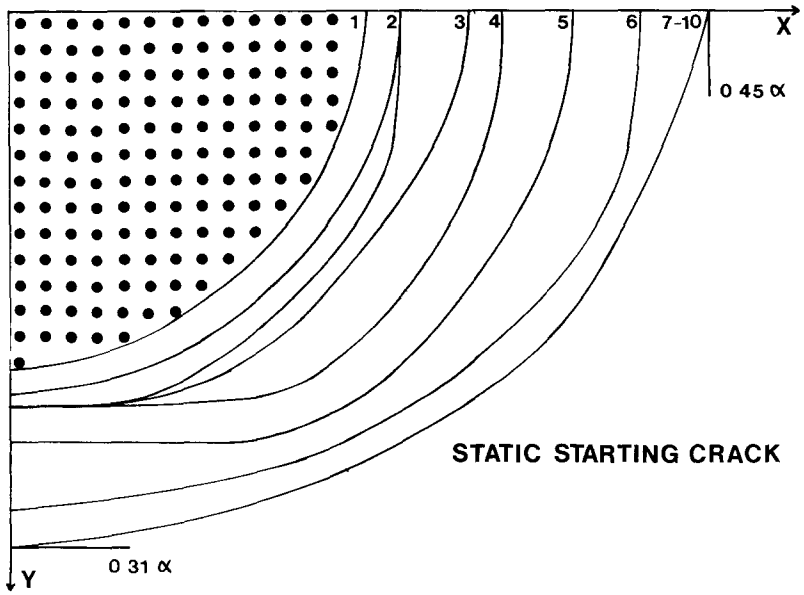

FIG 12 Rupture front motion for a spontaneous initially circular crack under static prestress loading. Dots indicate the preexisting crack, while lines show the rupture front at 10 different times starting from 0.4 with a step of 0.4. Rupture velocities are shown in the x and y directions, at the stopping time, once the crack has duplicated its initial length in the x direction

order to study the terminal velocity, we would need a much bigger grid and a much more expensive computation. In Figure 13, we present both the slip inside the crack and the stress field T_{xz} in the plane of the crack at several instants of time. ΔU_x and T_{xz} are shown as a function of radius along three directions: $\phi = 0°$ (x axis); $\phi = 45°$; and $\phi = 90°$ (y axis) to emphasize the nonsymmetrical nature of our solutions. The overall features of the slip and stress are, however, the same as those for the equivalent antiplane and in-plane problems. There is a slip deficiency in the initial preslipped section of the fault and there are inverse square-root singularities in stress outside the crack edge. The model presented here corresponds to a preslipped circular fault patch or asperity. The rupture then evolves from this preslipped segment which acts as a seed or trigger for the rupture. This model deserves a more careful analysis, in particular of nonsymmetrical rupture growth. This will be the subject of future work.

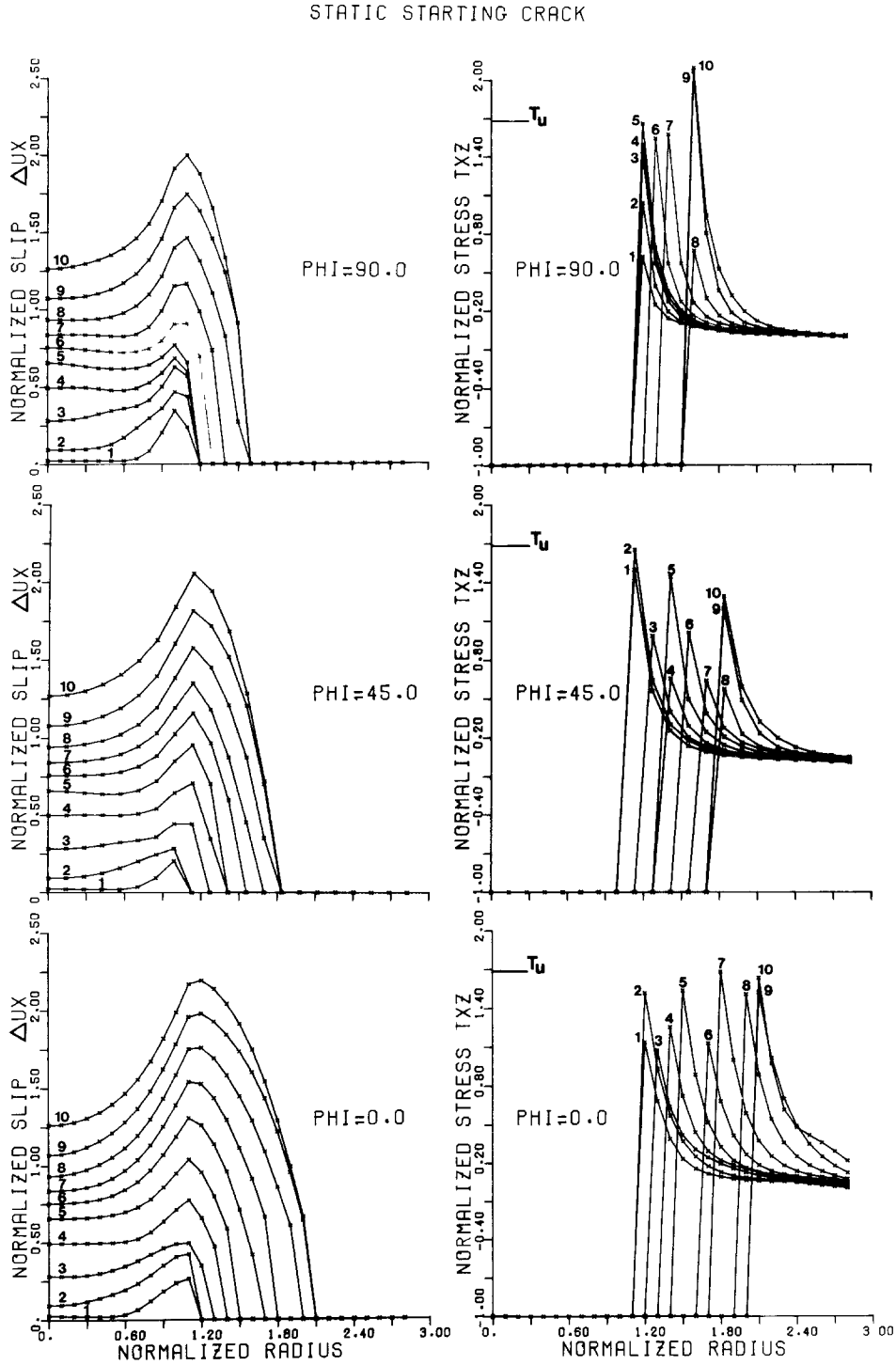

FIG. 13. Slip and stress fields along a line on the crack surface defined by its angle ϕ with respect to the x axis for the spontaneous rupture shown in Figure 12. Results are shown at 10 different times starting from 0.4 with a step of 0.4. T_u is the maximum stress associated with the static stress intensity K_I. The initial crack radius in the scale length

Instantaneously starting, spontaneous circular crack. The model we studied in the previous section is very expensive to solve, since it is necessary to calculate the initial static solution before rupture can start. Although we believe that this is the most realistic model of rupture nucleation, we shall study now a model of instantaneous nucleation. Models of this kind have been studied by Das (1981) and Miyatake (1980). In this model, a uniform preexisting stress field T_{xz} exists in the future fault zone. At time $t = 0$, a finite circular crack appears instantaneously with a radius $L = 10\ d$. For some time the stress intensity around the edge of the crack will increase until it reaches the rupture criterion which, as in the previous example, we shall assume to be $K_t = 0.42$. Rupture starts at normalized time $t_c = 0.12$ and then grows preferentially in the x direction. This is again a consequence of the stronger stress concentration in the in-plane mode dominating in the x direction. Figure 14 shows the shape of the rupture front as a function of time. Rupture is again stopped

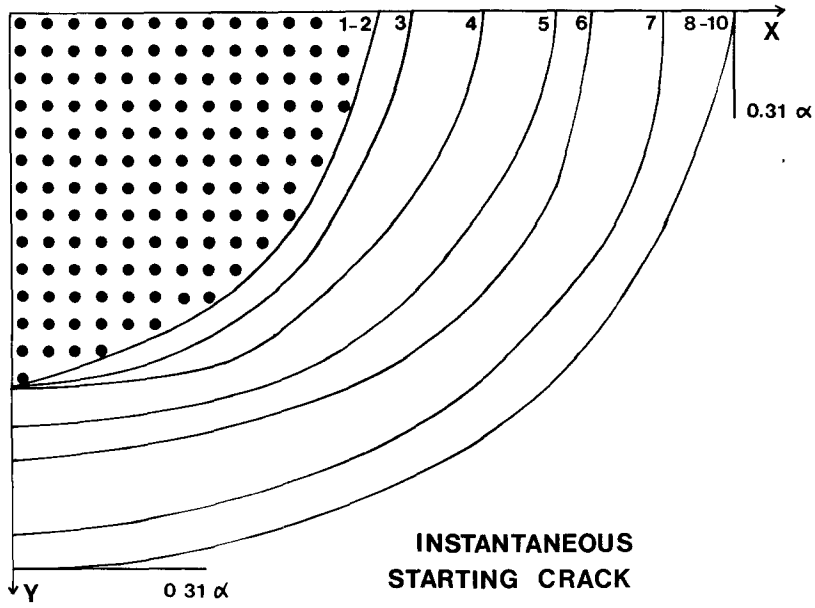

FIG. 14. Rupture front motion for a spontaneous initial circular crack under instantaneous stress loading. Dots indicate the initial crack at time $t = 0$, while lines show the rupture front at 10 different times starting from 0.5 with a step of 0.5 Rupture velocities are shown in the x and y directions, at the stopping time, once the crack has duplicated its initial length in the x direction.

abruptly once the crack has duplicated its half-length in the x direction; by that time, the crack has a clearly elliptical shape elongated in the x direction.

In Figure 15, we present the slip ΔU_x and stress T_{xz} at several instants of time. Cross section of slip and stress are shown as a function of radius in three azimuths: $\phi = 0°$ (x axis); $\phi = 45°$; and $\phi = 90°$ (y axis).

It is interesting to note that slip seems to stop at the center of the crack just before the crack starts growing. This occurs because the crack behaves as an instantaneous circular crack until it starts rupturing. For the instantaneous circular crack, slip arrest inside the crack starts with the arrival of the P waves generated at the edge of the crack at time $t = 0$. Slip restarts when the P waves generated by the start of rupture arrive. Between the arrival of these two waves, the slip decreases almost to a halt. At the end of rupture, once slip has stopped due to friction, slip inside the crack has the typical elliptical shape of static shear cracks.

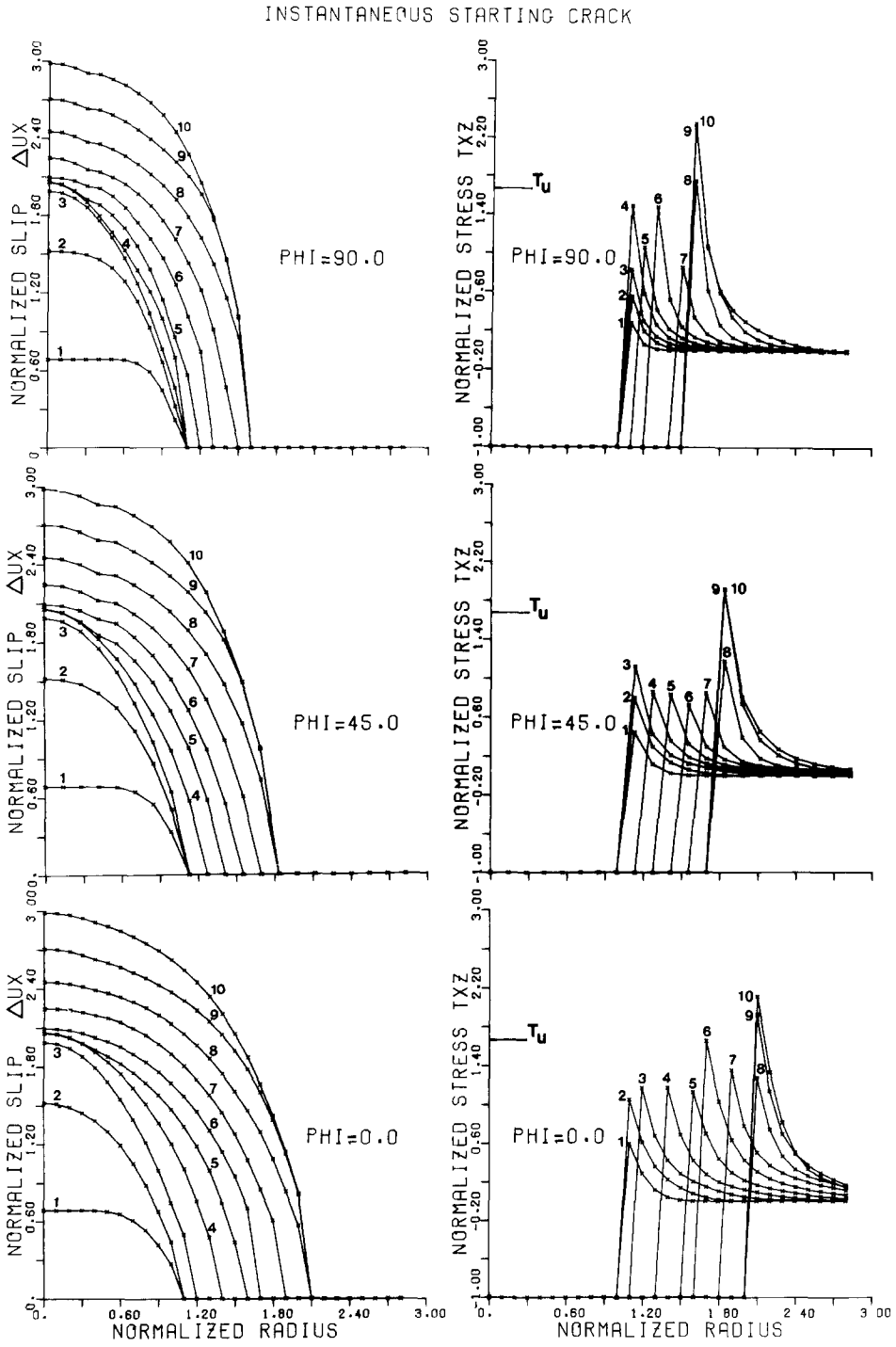

FIG 15. Slip and stress fields along a line on the crack plane defined by its angle ϕ with respect to the x axis for the spontaneous rupture shown in Figure 14 Results are shown at 10 different times starting from 0 4 with a step of 0.4 T_u is the maximum stress associated with the static stress intensity K_I. The initial crack radius is the scale length

CONCLUSIONS

In this paper, we have presented a general numerical technique to model the dynamic shear cracks at the origin of most shallow tectonic earthquakes. We have studied systematically two-dimensional antiplane and in-plane cracks, and three-dimensional initially circular cracks. In all three cases, we studied first fixed-rupture velocity models (semi-infinite or self-similar) for which partial or complete analytic solutions exist. We use these exact results as tests of our solutions and then verify carefully the stability of the stress field on the plane of the crack. We found very satisfactory results in most cases, noting a systematic underestimation of slip, due, in our opinion, to the fact that we do not calculate slip exactly on the crack but slightly off it. In the in-plane case, we verified that the numerical stress field cannot usually distinguish the rupture front singularity from the S-wave peak that closely precedes it at high rupture velocities. Once we were satisfied that the numerical stress field was stable enough, we attacked spontaneous rupture growth. The main problem is to provide a numerical criterion that approximates—at least qualitatively—the absorption of energy at the rupture front that controls crack growth. After a number of tests (Virieux, 1979), we decided to use the maximum stress criterion of Shmuely and Perets (1976) and Das and Aki (1977). In this criterion, the stress at the grid points immediately in front of the crack front are tested for a maximum value; if the stress is larger than this threshold, the crack front is advanced by a grid spacing. Any other rupture criterion will use the numerical fields calculated at a number of grid points in the vicinity of the rupture front. This will inevitably introduce numerical transients due to the finite time of propagation through the numerical mesh. The maximum stress criterion is the closest to an instantaneous criterion in the sense that the only numerical transient introduced will be due to the unknown position of the rupture front inside a numerical cell. The maximum stress criterion has also been used by Mikumo and Miyatake (1979), Day (1979), Das (1981), and Miyatake (1980). The maximum stress criterion has to be carefully analyzed if we want to translate it into physical terms and compare it to rupture criteria for the continuum. Das and Aki (1977) pointed out that the criterion is equivalent to a maximum stress intensity through a relation of the form

$$\sigma_u = \sigma_f + 2k_t d^{-1/2}. \tag{19}$$

It is clear, then, that implicit in the definition of the maximum there is a scale length that Das and Aki (1977) took as the grid spacing. If we want to translate the criterion into physical terms we have to adopt a value for the grid spacing d. After a careful dimensional analysis for a finite crack, we found that the proper scaling relation for the maximum stress, in terms of the nondimensional maximum stress intensity factor K_t, should be

$$\sigma_u = \sigma_f + 2\sigma_e K_t \sqrt{L/d}. \tag{20}$$

This emphasizes the role of crack length in any physically reasonable rupture criterion, this is a well-established result in fracture mechanics. Equation (20) shows that for a finite crack, the maximum stress criterion depends on the number of points inside the crack (L/d). The finer the discretization, the higher will be the value of σ_u for a given maximum stress intensity k_t. This property of the numerical solutions was not too evident in previous work on spontaneous rupture propagation

because of the way rupture was initiated. In these studies, rupture was initiated by an instantaneously appearing finite crack. In that case, the length scale is disguised in the time t_c during which the stress concentration around the crack edge builds up until it overcomes the rupture criterion. In order to keep low calculations costs, most authors have chosen very low values of the maximum stress so that t_c was very low and rupture accelerated very fast to transonic rupture velocities. Had they chosen larger values of the maximum stress, the crack would have waited a longer time to start growing, and it would (even) not have grown at all because the stress would have never overcome the rupture criterion. The maximum value of the calculated stress as shown in (20) depends on the number of points chosen inside the crack. The dependence on the fineness of the grid was clarified in this paper by the study of a more realistic form of crack nucleation: a finite preexisting crack becomes metastable at time $t = 0$, i.e., the stress just in front of the crack edge is larger than the maximum admissible stress. Rupture then starts to propagate and accelerate. In this case, it is obvious that the maximum stress has to be chosen lower than the maximum calculated stress if we want the crack to grow; in other words, the rate at which we sample the stress field in front of the rupture front will strongly influence the maximum calculated stress. Crack length is intimately related to the rupture criterion, a result that is very satisfying because all rupture criteria in fracture mechanics depend both on the state of stress and the size of the crack. This is a fundamental feature of both Irwin's and Griffith's fracture theories.

Acknowledgments

Part of this work was done while one of the authors (J. V.) visited the Lamont-Doherty Geological Observatory of Columbia University We thank Paul Richards for his support and comments on a first version of this paper. John Boatwright and Shamita Das provided very helpful discussions. We thank an unknown reviewer for his help in improving our original manuscript. While at Palisades, funds for computation were provided from the National Science Foundation Grant EAR 79-01810 In Paris, it was supported by the Institut National d'Astronomie et Géophysique through grants from A. T P. Géodynamique and A. T. P. Sismogenèse.

References

Alford, R. M., K. R. Kelly, and D. M. Boore (1974). Accuracy of finite-difference modelling of the acoustic wave equation, *Geophysics* **39,** 834–842.

Alterman, Z. S. and F C. Karal (1968). Propagation of elastic waves in layered media by finite difference methods, *Bull. Seism. Soc. Am.* **58,** 367–398.

Andrews, D. J. (1974). Evaluation of static stress on a fault plane from a Green's function, *Bull. Seism. Soc. Am.* **64,** 1629–1633

Andrews, D J. (1976). Rupture velocity of plane-strain shear cracks, *J. Geophys. Res.* **81,** 5679–5687.

Archuleta, R. J and S. M. Day (1980). Dynamic rupture in a layered medium the 1966 Parkfield earthquake, *Bull. Seism. Soc. Am.* **70,** 671–689.

Burridge, R. (1969). The numerical solution of certain integral equations with non-integrable kernels arising in the theory of crack propagation and elastic wave diffraction, *Phil Trans Roy. Soc. London, Ser. A* **265,** 353.

Burridge, R. and J. R. Willis (1969). The self-similar problem of the expanding elliptical crack in an anisotropic solid, *Proc Camb. Phil. Soc.* **66,** 443–468.

Das, S (1980). A numerical method for determination of source time functions for general three-dimensional rupture propagation, *Geophys. J.* **62,** 591–604.

Das, S. (1981). Three-dimensional spontaneous rupture propagation and implications for the earthquake source mechanism, *Geophys. J.* **67,** 375–394.

Das, S. and K. Aki (1977). A numerical study of two-dimensional spontaneous rupture propagation, *Geophys. J* **50,** 643–668.

Day, S. M. (1979). Three-dimensional finite difference simulation of fault dynamics, Final Report S^3 Project N° 12035, Systems, Science and Software, La Jolla, California.

Kostrov, B. V. (1964). Self-similar problems of propagation of shear cracks, *J. Appl. Math. Mech.* **28,** 1077–1087.

Kostrov, B. V. (1966). Unsteady propagation of longitudinal shear cracks, *J. Appl. Math. Mech.* **30,** 1241–1248.

Madariaga, R. (1976). Dynamics of an expanding circular fault, *Bull. Seism. Soc. Am.* **65,** 163–182.

Mikumo, T. and T. Miyatake (1979) Dynamical rupture process on a three-dimensional fault with non-uniform friction and near-field seismic waves, *Geophys J.* **54,** 417–438

Miyatake, T. (1980). Numerical simulations of earthquake source process by a three-dimensional crack mode. Part I. Rupture process, *J. Phys Earth* **28,** 565–598

Owen, D. R. J. and D Shantaram (1977) Numerical study of dynamic crack growth by the finite element method, *Int. J. Fracture* **13,** 821–837.

Popelar, C. H. and P. C. Gehlen (1979). Modelling of dynamic crack propagation. II Validation of two-dimensional analysis, *Int J. Fracture* **15,** 159–177.

Richards, P. G. (1973). The dynamic field of a growing plane elliptical shear crack, *Int. J. Solid Structures,* **9,** 843–861.

Richards, P. G. (1976). Dynamic motions near an earthquake fault a three-dimensional solution, *Bull Seism Soc. Am.* **66,** 1–32

Shmuely, M. and Z. S. Alterman (1973) Crack propagation by finite differences, *J. Appl Mech* **40,** 902–908.

Shmuely, M. and Peretz (1976) Static and dynamic analysis of the DCB problem in fracture mechanics, *Int. J. Solid Structures* **12,** 67–79.

Stockl, H (1977). Finite difference calculation of stress relaxation earthquake models, *J Geophys* **43,** 311–327.

Virieux, J. M. (1979). Etude numérique des modèles de failles à deux dimensions et des critères de propagation, *Thèse de 3ème Cycle,* Université de Paris VI, Paris, France.

LABORATOIRE D'ETUDE GÉOPHYSIQUE
DE STRUCTURES PROFONDES
INSTITUT DE PHYSIQUE DU GLOBE
UNIVERSITÉ DE PARIS VI
75230 PARIS CEDEX 05, FRANCE
CONTRIBUTION NO. 531

DÉPARTEMENT DE SCIENCES PHYSIQUES
DE LA TERRE
UNIVERSITÉ PARIS VII
PARIS, FRANCE

Manuscript received 17 December 1979